Water Research 95 (2016) 340–347

Contents lists available at ScienceDirect

Water Research

journal homepage: www.elsevier.com/locate/watres

Effect of foam on temperature prediction and heat recovery potential from biological wastewater treatment

L. Corbala-Robles, E.I.P. Volcke*, A. Samijn, F. Ronsse, J.G. Pieters

Department of Biosystems Engineering, Ghent University, Coupure Links 653, 9000 Ghent, Belgium

ARTICLE INFO

Article history:
Received 21 October 2015
Received in revised form
30 January 2016
Accepted 13 March 2016
Available online 16 March 2016

Keywords:
Foam
Heat balance
Heat recovery
Lab-scale experiment
Modeling
Simulation

ABSTRACT

Heat is an important resource in wastewater treatment plants (WWTPs) which can be recovered. A prerequisite to determine the theoretical heat recovery potential is an accurate heat balance model for temperature prediction. The insulating effect of foam present on the basin surface and its influence on temperature prediction were assessed in this study. Experiments were carried out to characterize the foam layer and its insulating properties. A refined dynamic temperature prediction model, taking into account the effect of foam, was set up. Simulation studies for a WWTP treating highly concentrated (manure) wastewater revealed that the foam layer had a significant effect on temperature prediction (3.8 ± 0.7 K over the year) and thus on the theoretical heat recovery potential (30% reduction when foam is not considered). Seasonal effects on the individual heat losses and heat gains were assessed. Additionally, the effects of the critical basin temperature above which heat is recovered, foam thickness, surface evaporation rate reduction and the non-absorbed solar radiation on the theoretical heat recovery potential were evaluated.

1. Introduction

The increasing scarcity of fossil energy resources and the need for reducing greenhouse gas emissions related to climate change have made renewable energy and energy efficiency an important issue in our society. Many efforts have been done to take advantage of the energy carried out by wastewater—from its point of generation to its point of treatment and discharge to the environment. Meggers and Leibungut (2011) and Cipolla and Maglionico (2014) studied the potential heat recovery from water in buildings. Dürrenmatt and Wanner (2014) developed a mathematical model to predict the effect of heat recovery on the wastewater temperature in sewers. In WWTPs, heat is an important resource which is generated during biological conversions and creates an opportunity for heat recovery from these systems, improving the energy use of the plant. The potential heat recovery increases with increasing biological heat production, i.e. for wastewater with high concentrations of organic matter and/or nitrogen. Nevertheless, activated sludge systems treating highly concentrated wastewater rarely operate at temperatures above 35–40 °C, which is rather low for practical applications. In order to increase the temperature of the available heat and so its usefulness, heat recovery from biological treatment processes can be performed with heat pumps (Hughes, 1984; Svoboda and Evans, 1987). The recovered heat could be applied to fulfill diverse heating requirements, e.g. heating of buildings and greenhouses.

To reliably estimate the heat recovery potential from a WWTP, a heat balance needs to be set up to calculate its temperature. The application of heat balances for the dynamic prediction of basin temperature has been demonstrated previously by, for example, Sedory and Stenstrom (1995) and Makinia et al. (2005). In another study, Gillot and Vanrolleghem (2003) compared two prediction models to obtain the equilibrium temperature in aerated basins which differed in their degree of complexity. Fernandez-Arevalo et al. (2014) presented a systematic methodology to incorporate heat transfer modeling in multi-phase biochemical reactors, enabling the dynamic description of mass and heat in a plant-wide context.

However, the influence of a foam layer on the heat balance of a WWTP has not been accounted for in literature so far. Foam formation is often observed on the surface of aeration basins of activated sludge systems, especially when treating concentrated wastewater. A foam layer can provide significant insulation

* Corresponding author.
E-mail addresses: Luis.CorbalaRobles@UGent.be (L. Corbala-Robles), Eveline.Volcke@UGent.be (E.I.P. Volcke), Samijn_Arne@hotmail.com (A. Samijn), Frederik.Ronsse@UGent.be (F. Ronsse), Jan.Pieters@UGent.be (J.G. Pieters).

http://dx.doi.org/10.1016/j.watres.2016.03.031
0043-1354/

(Cumby, 1987). Hughes (1984), for example, observed relatively high water temperatures in a large open topped lagoon during winter time and attributed these to the foam layer formed on the lagoon surface.

In this study, dedicated experiments were performed to characterize the foam and its insulating properties. The heat balance model was extended accordingly to account for foam formation on basin surfaces. The influence of foam on temperature prediction and on the heat recovery potential from a WWTP treating highly loaded wastewater was subsequently analyzed through simulation over a one-year period. A sensitivity analysis was performed to evaluate the influence of process parameters.

2. Materials and methods

2.1. Heat balance over a wastewater treatment basin

The heat balance (Eq. (1)) over a completely mixed basin with a constant volume V (m^3) expresses that heat accumulation, reflected by an increase of the basin temperature T_w (K) with time, t (s), results from advective heat transport H_{eff} (W) and the net heat exchange ΔH (W) over the basin.

$$\rho_w V c_{pw} \frac{dT_w}{dt} = H_{eff} + \Delta H \quad \left[J \cdot s^{-1} = W\right] \tag{1}$$

ρ_w (kg m^{-3}) denotes the density of the wastewater and c_{pw} (J kg^{-1} K^{-1}) its specific heat capacity. H_{eff} represents the heat required to bring the influent temperature (T_i) to the basin's temperature (T_w):

$$H_{eff} = \rho_w Q_w c_{pw} (T_i - T_w) \quad \left[J \cdot s^{-1} = W\right] \tag{2}$$

with Q_w (m^3 s^{-1}) the wastewater flow rate and T_i (K) the influent temperature. It was assumed that the density and specific heat capacity of the influent, basin and effluent were the same and constant through time. Furthermore, flow rate changes due to evaporation were neglected.

The net heat exchange (Eq. (3)) over the basin was represented by a sum of heat fluxes (see Fig. 1A):

$$\Delta H = H_{sr} + H_p + H_b - H_{ar} - H_{ev} - H_c - H_{tw} - H_{ae} - H_{hr} \quad \left[J \cdot s^{-1} = W\right] \tag{3}$$

where a positive or negative sign represents a heat gain or loss, respectively. The absorbed solar radiation (H_{sr}) was considered to be the available radiation on flat surfaces given in the typical reference year dataset from Belgium (Dogniaux et al., 1978). The power input (H_p) was derived from sub-surface aeration (Sedory and Stenstrom, 1995). The heat from biological reactions (H_b) comprised the heat from nitrification (H_{nit}), denitrification (H_{denit}) and organic degradation (H_{COD}). Atmospheric radiation (H_{ar}) was based on the Stefan-Boltzmann's law to describe the long-wave heat exchange between the basin and the sky. Surface evaporation (H_{ev}) and convection (H_c) were based on the dimensionless number analysis of forced convection in parallel flow over flat surfaces. Heat exchanges through the basin wall and bottom (H_{tw}) were calculated with an overall heat transfer coefficient. The sensible and latent heat lost due to aeration (H_{ae}) represents the heat required to bring aeration air to basin temperature and water evaporation as this airflow gets saturated (Sedory and Stenstrom, 1995). The heat recovery potential (H_{hr}) is the theoretical maximum surplus heat that can be removed from the basin while maintaining an appropriate reaction temperature (T_{crit}). It should be noted that the abovementioned heat losses, exempting H_{hr}, can become heat gains when the environment is at a higher temperature than the system. The complete set of equations is presented in the Supplementary Material, Table S1.

The heat generated during nitrification (H_{nit}) and denitrification (H_{denit}) was calculated taking into account biomass growth, based on the yield coefficients given by (Wiesmann, 1994), as $H_{nit} = 18.9$ MJ $kg_{NH4\text{-}N}^{-1}$ and $H_{denit} = 41.3$ MJ $kg_{NO3\text{-}N}^{-1}$ (at 25 °C, see Supplementary material S1). The heat from organic matter degradation (H_{COD}) originates from the aerobic removal of chemical oxygen demand (COD). To correctly account for the heat generation from organic matter degradation, transformations such as hydrolysis and CO_2 stripping taking place simultaneously need to be considered; they are implicitly included in experimental estimations of heat of reactions (Fernández-Arévalo et al., 2014). Therefore, the value for heat released by organic matter degradation was taken from Blackburn and Cheng (2005), who found a heat production of 13.9 MJ kg_{COD}^{-1} when processing high strength swine waste.

2.2. Foam layer modeling

The heat supplied by the basin to the upper surface of the foam layer (H_f) was assumed to be in equilibrium with the heat lost to the environment at the foam surface (Eq. (4) and Fig. 1B), this considering the small heat capacity of the outermost part of the foam layer in contact with the environment.

$$H_f = H_{ar} + H_{ev} + H_c \quad \left[J \cdot s^{-1} = W\right] \tag{4}$$

The heat exchange via atmospheric radiation (H_{ar}), evaporation

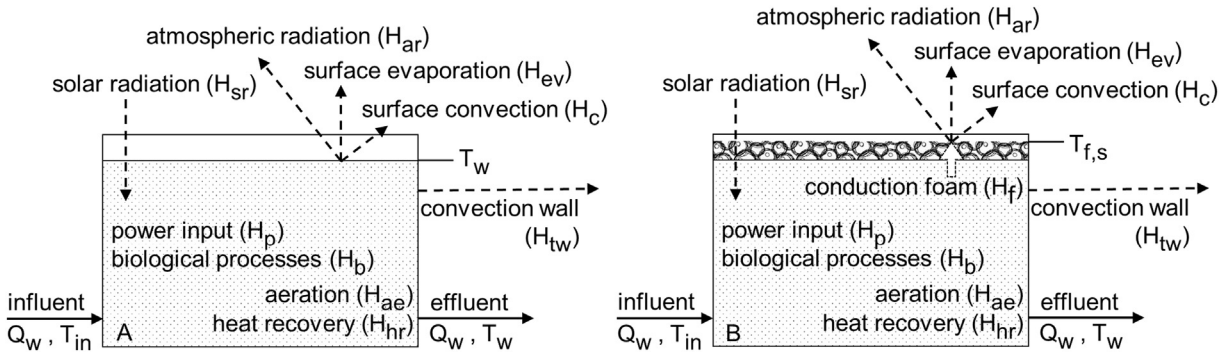

Fig. 1. Heat fluxes acting on an aeration basin: (A) without foam; (B) with foam, where the heat exchanged by the basin to the upper surface of the foam layer (H_f) is equal to the heat exchanged with the environment at the surface (H_{ar}, H_{ev} and H_c).

(H_{ev}) and surface convection (H_c) depends on the surface temperature of the basin. In the presence of a foam layer, this temperature is not the aeration basin temperature (T_w) but the foam's surface temperature ($T_{f,s}$) (Fig. 1B). The temperature difference between the aeration basin and the foam surface is a function of the insulating capacity of the foam layer, which is assumed here to increase proportionally to the foam thickness, d (m), and inversely to its apparent conductivity, λ_{foam} (W m^{-1} K^{-1}). This insulating capacity influences the heat flow through the foam layer (H_f) depending on the temperature difference within the foam and the basin surface area:

$$H_f = \frac{\lambda_{foam} A}{d}\left(T_w - T_{f,s}\right) \quad \left[J \cdot s^{-1} = W\right] \tag{5}$$

The atmospheric radiation (H_{ar}; Eq. (6) in Table 1) was implemented considering the sky as a black body (emissivity, $\varepsilon_{sky} = 1$) and its radiative temperature calculated according to Swinbank (1963). For this model refinement, it was supposed that for a totally overcast sky the radiative sky temperature (T_{sky}) equals the air temperature (Pieters et al., 1995) (Eq. (7) in Table 1). Previous studies, such as Talati and Stenstrom (1990) (Eq. (8) in Table 1), require the calculation of the atmospheric radiation factor (β) to calculate atmospheric radiation. This factor is a function of the cloud cover and vapor pressure (Raphael, 1962; Talati, 1988). An analysis has been made to evaluate the effect of this refinement on temperature prediction.

Further refinements of previous models (Sedory and Stenstrom, 1995; Talati and Stenstrom, 1990) were implemented in this study to calculate surface evaporation (H_{ev}) and convection (H_c) based on dimensionless number analysis (Eqs. (9) and (11) in Table 1, respectively), as studied in the steady state model by Lippi et al. (2009). The effect of these changes on the dynamic temperature prediction were assessed.

Foam formation can reduce surface evaporation in two ways. First, due to the foam's insulating properties, the basin surface temperature (i.e. the foam surface) is lower than the basin temperature, therefore reducing the driving force of water evaporation. Second, it can reduce the evaporation rate from the basin surface (Frenkiel, 1965). The former is a direct outcome from considering the foam as an insulating layer in the model (Eqs. (4) and (5)). To assess the effect of the latter on the heat recovery potential, a parameter representing the possible evaporation rate reduction due to the foam layer has been added to the model (R_{ev}; Eq. (9) in Table 1).

The amount of solar radiation absorbed by the basin (H_{sr}) depends on the total available solar radiation ($H_{sr,TRY}$; obtained from Belgium's typical reference year dataset (Dogniaux et al., 1978)), site-specific factors (i.e. shading and reflection by adjacent buildings and landscape) and the fraction of solar radiation reflected by the basin's surface. To evaluate the effect of this possible "loss" of the available solar radiation on heat recovery, a parameter was added for the solar radiation calculation (ρ′; Eq. (14) in Table 3), which represents a fraction from the available solar radiation that would not be absorbed by the basin.

2.3. Simulation set-up

A reference scenario (RS) was defined corresponding with a foam layer thickness of d = 0.17 m, without heat recovery ($H_{hr} = 0$). This scenario considered that the absorbed radiation equaled the available radiation (ρ' = 0; Eq. (14) in Table 3) and did not have any evaporation rate reduction due to the foam layer ($R_{ev} = 0$; Eq. (9) in

Table 2
Basin and average influent characteristics for the plant under study.

Symbol	Characteristic	Value	Unit
V	Basin volume	2846	m^3
A	Basin surface area	547	m^2
h_{basin}	Basin depth	5.2	m
	Wall thickness	0.3	m
N	Amount of aerators	68	–
P_{aer}	Aerator power	809	W
η	Aerator efficiency	75	%
Q_w	Influent	57.9	m^3 d^{-1}
Q_{air}	Aeration flow	1360	m^3 h^{-1}
S_{COD}	Organic load	30	Kg COD m^{-3}
	Organics removal efficiency	90	%
$S_{NH4\text{-}N}$	Nitrogen load	4.5	Kg NH_4-N m^{-3}
	Nitrogen removal efficiency	88	%

Table 1
Model refinements: equations proposed by Talati and Stenstrom (1990) and the ones applied in this study (in bold font). The assessment of the effect of these refinements on temperature prediction was evaluated with three different cases: I) atmospheric radiation; II) surface evaporation and convection; III) case I and II combined (Table S3).

Equations	Eq.	Parameter		
		Symbol	Description	Unit
Atmospheric radiation (cases I & III)				
$\boldsymbol{H_{ar} = \varepsilon_{f,s}\sigma A T_{f,s}^4 - \varepsilon_{sky}\sigma A T_{sky}^4}$	6	$\varepsilon_{f,s}$	basin surface emissivity	Fraction
		σ	Stefan Boltzmann constant	W m^{-2} K^{-4}
$\boldsymbol{T_{sky} = \frac{C_c}{10} T_{air} + \left(1 - \frac{C_c}{10}\right)\left(0.0522 \cdot T_{air}^{1.5}\right)}$	7	C_c	cloud cover	Tenths
		T_{sky}	sky radiative temperature	K
$H_{ar} = \varepsilon_{f,s}\sigma A T_{f,s}^4 - (1-\lambda)\beta\sigma A T_{air}^4$	8	λ	water reflectivity	Fraction
		T_{air}	ambient air temperature	K
		β	atmospheric radiation factor	Dimensionless
Surface evaporation (cases II & III)				
$\boldsymbol{H_{ev} = (1 - R_{ev})\frac{D_{w,a}}{L} 0.037 Re^{\frac{4}{5}} Sc^{\frac{1}{3}} A\left(C^*_{T,f,s} - C^{\infty}_{T,air}\right) h_{lat}}$	9	R_{ev}	evaporation rate reduction due to the foam	Fraction
		$D_{w,a}$	diffusivity coefficient of water vapor in air	m^2 s^{-1}
$H_{ev} = \frac{4.18}{3600 \cdot 24}\left(1.145 \cdot 10^6\left(1 - \frac{r_h}{100}\right) + 6.86 \cdot 10^4 (T_{f,s} - T_{air})\right) e^{0.0604 T_{air}} W A^{0.95}$	10	L	basin diameter	m
		$C^*_{T,f,s,}$	saturated vapor density at surface temperature	kg m^{-3}
		$C^{\infty}_{T,air}$	ambient air vapor concentration	kg m^{-3}
		h_{lat}	latent heat of evaporation	J kg^{-1}
		r_h	relative humidity	%
		W	wind speed	m s^{-1}
Surface convection (cases II & III)				
$\boldsymbol{H_c = \frac{\lambda_{air}}{L} 0.037 Re^{\frac{4}{5}} Pr^{\frac{1}{3}} A(T_{f,s} - T_{air})}$	11	λ_{air}	air thermal conductivity	W m^{-1} K^{-1}
$H_c = \rho_{air} c_{pa,air} h_v A(T_{f,s} - T_{air})$	12	h_v	vapor phase transfer coefficient	m s^{-1}

Table 3
Sensitivity analysis of the effect of different parameters on the heat recovery potential. The reference scenario with heat recovery (RS_{hr}) is presented in bold. A critical temperature T_{crit} = 293.15 K has been used in all the presented scenarios.

Tested parameter		Tested value	Theoretical heat recovery potential (MWh year^{-1})	Relative to RS_{hr} (%)
Foam thickness (d)		0.00 m	644	−30
$H_f = \frac{\lambda_{foam} A}{d}(T_w - T_{f,s})$	Eq. (5)	0.01 m	663	−28
		0.10 m	819	−11
		0.17 m	**922**	**0**
Surface evaporation rate reduction (R_{ev})		**0%**	**922**	**0**
$H_{ev} = (1 - \boldsymbol{R_{ev}}) \frac{D_{w,a}}{L} 0.037 Re^{\frac{4}{5}} Sc^{\frac{1}{3}} A(C^*_{T,f,s} - C^{\infty}_{T,air}) h_{lat}$	Eq. (9)	30%	1009	9
		60%	1128	22
		90%	1278	39
Non-absorbed fraction from the available solar radiation (ρ′)		**0%**	**922**	**0**
$H_{sr} = (1 - \boldsymbol{\rho'}) \cdot A \cdot H_{sr,TRY}$	Eq. (14)	25%	809	−12
		50%	692	−25
		75%	590	−36
		100%	486	−47

Table 1). The effect of the foam layer on the one hand and possible heat recovery on the other hand on temperature prediction and on the heat fluxes were addressed separately. For this purpose, two additional scenarios were defined, with the same parameters d, R_{ev} and ρ′ as RS: a scenario with no foam and no heat recovery (RS_{nf}; d = 0 m) and a scenario including both a foam layer and heat recovery (RS_{hr}; d = 0.17 m). For the latter, a critical temperature (T_{crit} = 293.15 K) was defined and the heat recovery potential was considered to be the surplus heat that could be removed from the basin while maintaining this temperature, provided enough heat was produced. A sensitivity analysis was performed on RS_{hr} to assess the influence of the foam thickness, evaporation rate reduction and the non-absorbed fraction from the available solar radiation on the heat recovery potential. An overview of the performed simulations is presented in the supplementary information (Table S3).

The dynamic basin temperature profile $T_w(t)$ was obtained from Eq. (1), in which H_{tw}, H_{ae} and H_{hr} are functions of T_w, and considering Eqs. (4) and (5) to deal with H_{ar}, H_{ev}, and H_c. The corresponding equations were implemented in MATLAB (MATLAB, R2014a). The Euler method was used as integration technique, the initial basin temperature was taken as 288.15 K (15 °C). Changes in weather conditions (e.g. cloud cover, solar radiation and air temperature) and other input variables (e.g. influent temperature and ground temperature) have been accounted for on a half-hour basis. For the influent and ground temperatures, this has been done through linear interpolation of monthly averaged values. The time step considered in the integration was half an hour.

2.4. Wastewater treatment plant under study

The wastewater treatment plant under study concerned a typical installation in Flanders, Belgium, treating the liquid fraction of manure after centrifugation. This installation comprises COD and nitrogen removal through activated sludge in a pre-denitrification system. Because of the high influent organic carbon and ammonium concentrations, the temperature in these systems rises to such extent that cooling is often required during summer to avoid hampering of biological activity due to high temperatures. The main plant characteristics are summarized in Table 2. The meteorological data were obtained from the typical reference year dataset from the Royal Meteorological Institute of Belgium (Dogniaux et al., 1978).

2.5. Experimental determination of the foam characteristics

Dedicated experiments were performed to determine the temperature profile within the foam layer, its apparent thermal conductivity (λ_{foam}) and the influence of the aeration flow rate on these characteristics. The aeration basin was simulated by a tube (outer diameter = 0.110 m; inner diameter = 0.105 m; height = 1.5 m) which was well insulated such that it could be assumed that heat loss only took place through the surface. Two tubes were operated in parallel, in one of which mineral oil was added as an anti-foaming agent. In the other tube, foam was formed due to aeration up to a foam level of 0.17 m. All tests were carried out using wastewater from a pig manure WWTP (Trevi N.V.). Before each test, the wastewater was heated to over 303 K, to simulate the temperatures achieved in aerobic biological treatments and thus create a significant temperature difference in the basin compared to the environment. Aeration was provided by aquarium pumps (Rena® Air 200); the aeration flow rate was kept constant at 76 L h^{-1}.

A linearity test was conducted to determine whether the temperature of the foam layer changes linearly with the foam thickness. The temperature profile within the foam layer was determined based on measurements from three thermocouples (Type T; 0.5 °C accuracy) at position 0.096 m, 0.117 m and 0.172 m, where 0 m represents the foam surface in contact with ambient air. An Agilent 34970A Data Acquisition/Data Logger Switch Unit was used to register the temperature from each thermocouple every 5 s. The test lasted approximately 7 h, in order to ensure the foam to be in thermal equilibrium. The different temperature profiles throughout the foam layer were then obtained with the average value from 500 measurements (representing 42 min) of each thermocouple.

Experiments were carried out to investigate the effect of the aeration flow rate (ranging from 40 L h^{-1} to 110 L h^{-1}) on the heat resistance, under atmospheric as well as laboratory conditions, with and without foam layer. Each test consisted of 500 measurements (5 s interval in between), creating a dataset for each flow rate representing approximately 42 min.

3. Results and discussion

3.1. Foam layer characterization based on experimental results

3.1.1. Temperature profile within foam layer

The temperature gradient throughout the foam was uniform for the duration of the experiment (approx. 7 h) (Fig. 2). This indicates that the foam can be modeled as an insulating layer with conductive heat loss characterized by an apparent thermal conductivity (λ_{foam}). The insulating capacity of the foam layer thus increases in proportion to its thickness.

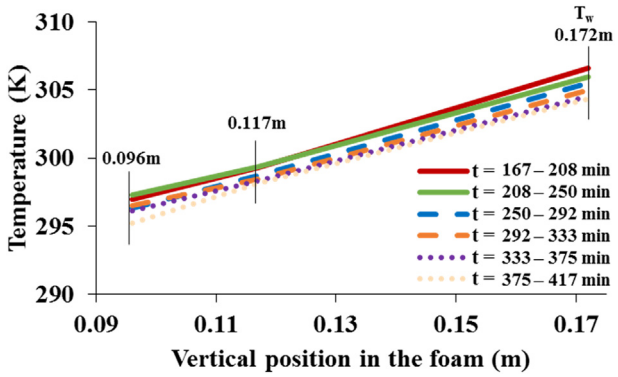

Fig. 2. Temperature profile within foam layer, based on measurements at different time instants at positions 0.096 m, 0.117 m and 0.172 m, where 0 m represents the foam surface in contact with ambient air. Each point represents the average temperature measured in that time period.

3.1.2. Influence of aeration flow rate

The effect of the aeration flow rate (40–110 L h^{-1}) on the heat resistance of the foam layer was negligible, both under atmospheric and laboratory conditions and with and without foam layer (results not shown).

3.1.3. Thermal conductivity coefficient of the foam layer

Given that the aeration flow rate did not influence the thermal conductivity coefficient of the foam layer, its value could be calculated from the experimental data from the temperature profile tests (Fig. 2). It was assumed that the heat loss during these tests only took place through the surface and as such needed to pass through the foam layer:

$$H_f = V \cdot \rho_w \cdot c_{p,w} \frac{T_w(t) - T_w(t_0)}{t - t_0} \quad \left[J \cdot s^{-1} = W\right] \tag{13}$$

where t and t_0 (s) are the start and end time of data registration, respectively. Substituting Eq. (13) in Eq. (5) and considering that the ratio (T_w-$T_{f,s}$) d^{-1} [K m^{-1}] in the latter equation is the slope of the graph shown in Fig. 2 yields the apparent thermal conductivity coefficient of the foam layer (λ_{foam}). The average value of this coefficient was determined as 13 W m^{-1} K^{-1} and implemented in the model.

It is important to note that this apparent thermal conductivity was found for a relatively stable foam layer using the thin fraction of swine manure as wastewater and subsurface aeration. Different values can be encountered with different wastewaters or activated sludge (depending on the solids content, surfactants, etc.). Furthermore, different types of aeration could not only affect the basin's temperature (Talati and Stenstrom, 1990), but also the properties and stability of the foam layer formed.

3.2. Temperature prediction and heat fluxes for the reference scenario (RS)

The predicted temperature profiles of the basin (T_w) and the foam surface ($T_{f,s}$) when no heat recovery ($H_{hr} = 0$) is applied are shown in Fig. 3A, comparing the reference scenario (RS) to a scenario with no foam (RS_{nf}). The basin temperature is the highest in the period May - October (days 120–270), peaking in June (days 150–180). When considering the average temperature per day, the foam surface temperature was 9.4 ± 2.5 K higher than the air temperature and 5.2 ± 1.0 K lower than the basin temperature, corresponding with a total temperature difference between the basin and the air of 14.5 ± 2.7 K for RS. When no foam layer is present (RS_{nf}), the temperature difference between the basin and the air is only 10.7 ± 2.8 K. Therefore, the basin temperature predicted when foam is considered is 3.8 ± 0.7 K higher than in the scenario without foam. Foam layer insulation in basins has thus an important impact on the temperature prediction and should be considered when modeling aeration basins where foam formation is expected.

A direct comparison between the heat gains, i.e. solar radiation (H_{sr}), power input (H_p) and biological reaction heat ($H_b = H_{nit} + H_{denit} + H_{COD}$), and the heat losses, i. e atmospheric radiation (H_{ar}), surface evaporation (H_{ev}), surface convection (H_c), heat exchange through wall and bottom (H_{tw}), aeration (H_{ae}) and advective heat transport (H_{eff}) is displayed in Fig. 4A. The heat from biological reactions (H_b) was the major heat gain in the system, accounting for 78% of the total heat gain (46% from organic matter removal, 22% from denitrification and 10% from nitrification). The most significant heat losses in the system occurred through the surface of the basin (H_{ar}, H_{ev} and H_c) accounting for 72% of the total heat loss throughout the year. From these heat losses, surface evaporation was the largest (35% from the total heat loss). This reiterates the importance of accounting for a foam layer, since it affects the temperature gradient between the environment and the basin surface which drives these heat losses (Fig. 3A).

The largest heat gains and losses were obtained in June. During this month, the highest values for solar radiation (H_{sr}) and heat required to bring the influent up to basin temperature (H_{eff}) are obtained. During winter periods, evaporation (H_{ev}) and atmospheric radiation (H_{ar}) heat losses have their lowest values (December and January). Also note that the influent nitrogen and organic matter were assumed constant over the year and so was their removal rate, resulting in a constant (average) heat generated by biological reactions and by the (aeration) power input.

3.3. Heat recovery potential and influence on heat fluxes (RS_{hr})

The dynamic temperature profile in case all heat above the critical temperature T_{crit} = 293.15 K was withdrawn, is shown in Fig. 3B. Heat was recovered from March to November (days 80–330), i.e. about 70% of the year. Surface heat losses (H_{ar}, H_{ev} and H_c) represented 49% of the total heat loss throughout the year. From these, atmospheric radiation and surface evaporation were the greater contributors with 21% and 18%, respectively. The theoretical heat recovery potential (H_{hr}) accounted for 35% of the total heat loss throughout the year.

The implementation of heat recovery (H_{hr}) lead to the decrease of the basin (T_w) and foam surface ($T_{f,s}$) in comparison to the reference scenario (Fig. 3B). As a result, the air temperature (T_{air}) sometimes exceeds both the surface and basin temperatures, turning some heat losses into heat gains (i.e.H_{ar}, H_{ev}, H_c, H_{tw} and H_{ae}). Surface heat convection (H_c), for example, represented less than 1% of the total heat loss during the month of June. This, in contrast to the reference scenario without heat recovery ($H_{hr} = 0$), where surface heat convection heat losses represented 11% of the total heat loss during the same month (Fig. 4). During this same month, the total heat losses (excluding H_{hr}) were reduced by 66% in comparison to the reference scenario.

The heat recovery potential depends directly on the selected critical temperature for heat extraction. The theoretical heat recovery potential corresponding with a critical temperature (T_{crit}) of 293.15 K was 922 MWh per year. Increasing this temperature decreased the amount of heat that can be recovered from the system (Fig. 5). On the one hand, if the critical temperature was increased by 5 K, the heat potential was reduced to 407 MWh per year (56% reduction). On the other hand, a 5 K reduction of the

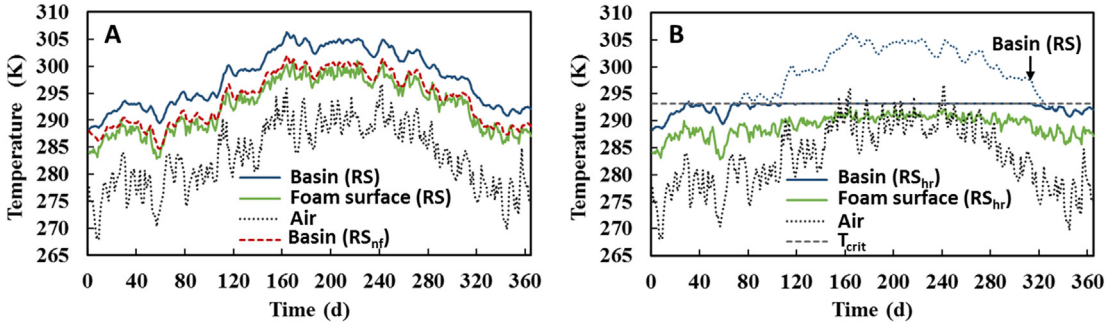

Fig. 3. Temperature prediction (daily averages) over one year: (A) no heat recovery considered ($H_{hr} = 0$); (B) considering the theoretical maximum heat recovery from the system ($T_{crit} = 293{\cdot}15$ K).

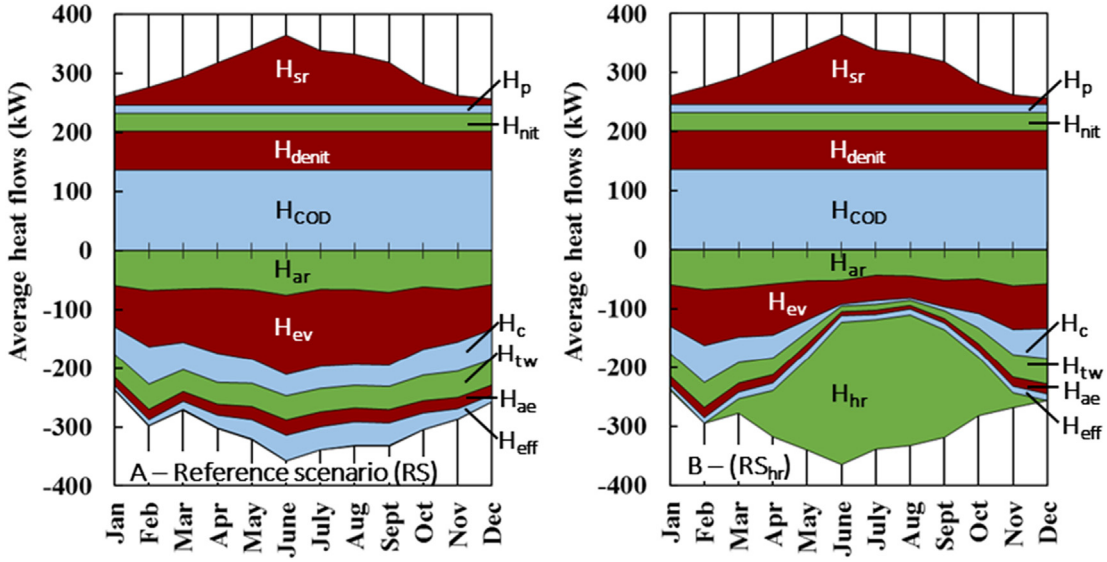

Fig. 4. Heat flux breakdown over a one-year period (monthly averages): (A) without heat recovery ($H_{hr} = 0$); (B) with heat recovery from the system.

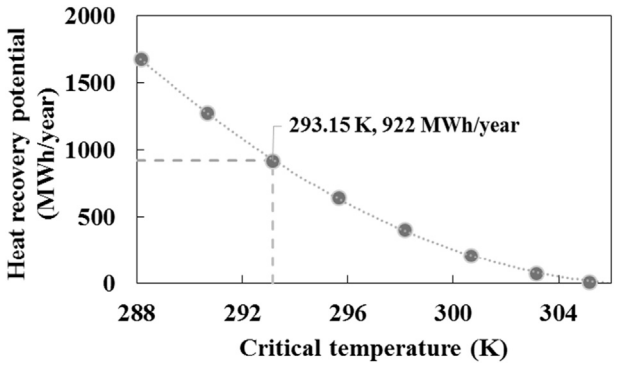

Fig. 5. Heat recovery potential as a function of the chosen critical temperature.

critical temperature yields an 82% higher heat recovery potential. The critical temperature has to be chosen as low as possible to maximize the heat recovery but high enough to ensure sufficient biological activity in terms of carbon and nutrient removal.

3.4. Effect of model refinements on the dynamic temperature prediction

The effect of the proposed model refinements (Table 1 and Table S3) on the dynamic temperature prediction for the reference scenario (including a foam layer and without heat recovery) was evaluated with three cases: (I) Comparison of equations to describe atmospheric radiation (H_{ar}; Eq. (6) versus Eq. (8) in Table 1). (II) Comparison of equations to describe surface evaporation and convection (H_{ev} and H_c, Eqs. (9) and (11) versus 10 and 12 in Table 1, respectively). (III) Combined effect of (I) and (II).

The equation proposed to calculate atmospheric radiation (Eq. (6) in Table 1) results in a lower temperature prediction (0.4 ± 0.2 K lower throughout the year) compared to the temperature predicted when Eq. (8) is used (Fig. 6 – I). The proposed equation predicts a higher heat loss through atmospheric radiation (4% higher in average throughout the year). This model refinement had a smaller effect on temperature prediction in comparison to that of case II (64% smaller temperature difference) and in the opposite direction (lower instead of higher temperature prediction when the proposed model is used) (Fig. 6).

Applying the equations based on dimensionless number analysis proposed in this study to describe surface evaporation and convection (Eqs. (9) and (11) in Table 1) resulted in a higher basin

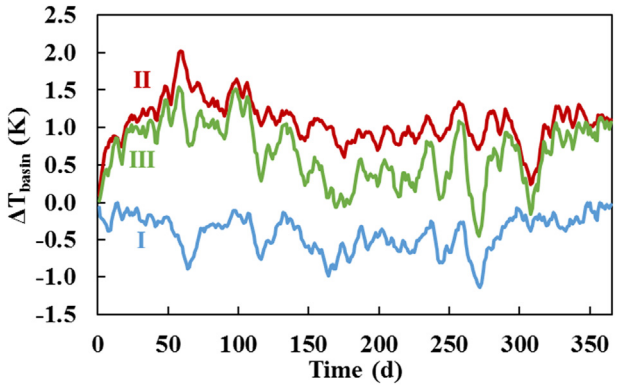

Fig. 6. Comparison of dynamic basin temperature prediction (daily averages) between models applied in this and in previous studies. A positive value indicates a higher temperature predicted by the proposed model.

temperature prediction (1.1 ± 0.3 K higher throughout the year) in comparison to the temperature predicted with the equations proposed in previous studies (Eqs. (10) and (12) in Table 1) (Fig. 6 – II). This temperature difference resulted from the higher heat loss predicted by Eqs. (10) and (12) in comparison to the ones proposed in this study (Eqs. (9) and (11) in Table 1). The heat flux predicted by Eqs. (10) and (12) increased the total heat loss from the basin 13% on average throughout the year. The equations used previously to describe these surface heat losses originate from the work of Harbeck Jr. (1962) and Novotny (1973). These studies used mass-transfer coefficients obtained for natural large water reservoirs with surface areas ranging from 4×10^3 to 1.2×10^8 square meters and without external heating in the form power input or elevated heat generated from biological reactions. The area of the simulated aeration basin is almost four times smaller than the lowest range value from these studies ($A = 547\ m^2$), which might be the origin of the higher heat flux predicted by these equations (and mass-transfer coefficients).

When all model refinements (for H_{ev}, H_c and H_{ar}) are considered (case III), the temperature predicted by the equations used in this study (Eqs. (6), (9) and (11)in Table 1) is 0.7 ± 0.4 K higher throughout the year (Fig. 6 – III). This resulted from the counteracting effects of the equations proposed for surface evaporation and convection to the effect of the equation proposed for atmospheric radiation.

3.5. Sensitivity analysis

Foam thickness had an important effect on the theoretical heat recovery potential of the system (Table 3). The heat recovery potential varied linearly in proportion to this thickness. If no foam was considered in the system, the theoretical heat recovery potential decreased by 30% in comparison to the reference scenario with heat recovery (RS_{hr}; foam thickness = 0.17 m). Foam control can play a major role in wastewater treatment operation in terms on temperature control and maximization of the heat recovery potential. Allowing thicker foams can potentially help sustain thermophilic basin temperatures.

Surface evaporation rate reduction (R_{ev}) can potentially increase the theoretical heat recovery by 39% (for the simulated system) if the rate is reduced by 90%. This effect is more pronounced when the critical temperature increases, since higher temperatures translate into higher surface evaporation heat losses. For instance, if a critical temperature 5 K higher is chosen (i.e. $T_{crit} = 298.15$ K), the theoretical heat recovery potential increases by 80% when an evaporation rate reduction $R_{ev} = 90\%$ is used. Surface evaporation rate reduction has been studied in the presence of surface oily layers (Frenkiel, 1965). Reductions up to 85–90% have been observed in some studies (Heymann and Yoffe, 1942, 1943; Shukla et al., 1962) but specific information on the effect of the foam layer in aeration basins treating the thin fraction of manure on evaporation reduction is still lacking. Future work on the characterization of foam layers could improve significantly the temperature prediction capabilities and improve process design, especially in thermophilic processes in which higher temperatures, and thus higher evaporation rates, are expected.

If a fraction of the solar radiation is not absorbed by the basin, the heat recovery potential of the system decreases (less heat enters the system). In the most extreme scenario, in which no solar radiation is absorbed, the theoretical heat recovery potential decreased by 47%. As mentioned earlier, the main two factors affecting the fraction of solar radiation that is not absorbed are shadowing effects (e.g. by adjacent buildings) and the reflectivity of the foam surface (albedo). In order to account for these factors, further in-site measurements and foam characterizations would need to be carried out, but this falls out of the scope of this contribution.

For water bodies, reflectivity is high when solar radiation is low (during the early morning and late afternoon) when the sun is closer to the horizon and low (3–10%; Oke (1992)) when solar radiation is high (sun further from the horizon). Therefore, for cases dealing with surfaces that behave like water (in terms of its reflectivity), the effect of the albedo in temperature and heat recovery prediction is expected to be small.

4. Conclusions

A heat balance was set up considering the effect of a foam layer on a wastewater treatment basin on its temperature profile and on the resulting heat recovery potential.

- The basin temperature is clearly dependent on the insulating capacity of the foam (ratio between its thickness and its apparent conductivity). Thicker foams will result in smaller surface heat losses and therefore higher basin temperatures and heat recovery potentials. When present, foam layers should clearly be accounted for in temperature prediction models.
- Experimental results indicated that the temperature gradient is uniform throughout the foam layer, once steady state is reached. The foam can be thus characterized by an apparent thermal conductivity coefficient (λ_{foam}), which was found to be 13 W m^{-1} K^{-1} and was not affected by the aeration flow rate.
- Heat recovery from wastewater treatment plants can play a major role to increase their efficiency. For a WWTP treating 58 m^3 d^{-1} of the thin fraction of manure (30 kg COD m^{-3}; 4.5 kg NH_4-N m^{-3}), a theoretical heat recovery potential of 922 MWh per year was calculated, demonstrating the potential of heat recovery from systems treating highly concentrated wastewater.
- The effect of model refinements to calculate atmospheric radiation, surface evaporation and convection on the dynamic temperature prediction was assessed. The largest effect, 1.1 K as yearly average, resulted from the calculation of surface evaporation and convection using dimensionless number analysis.
- There are clear seasonal effects on the heat fluxes and the resulting heat recovery potential. Heat loss through surface evaporation showed the largest changes throughout the year, being at its highest in June and at its minimum in January-December. The overall heat recovery potential was clearly higher in summer than in winter.
- Sensitivity analyses revealed a significant effect of foam thickness, surface evaporation rate reduction and non-absorbed solar

radiation on the heat recovery potential. For a correct inclusion of these parameters, site/process specific characteristics must be considered.

Acknowledgements

The authors thank Eddy Philips for his assistance with the experimental work. Trevi N.V. is acknowledged for providing the wastewater used for the experiments as well as full-scale process data. Luis Corbala-Robles work was supported by the Ghent University Special Research Fund through a Doctoral Scholarship (Grant Number: BOF14/DOC/046).

Appendix A. Supplementary data

Supplementary data related to this article can be found at http://dx.doi.org/10.1016/j.watres.2016.03.031.

References

Blackburn, J.W., Cheng, J., 2005. Heat production profiles from batch aerobic thermophilic processing of high strength swine waste. Environ. Prog. 24 (3), 323–333.
Cipolla, S.S., Maglionico, M., 2014. Heat recovery from urban wastewater: analysis of the variability of flow rate and temperature. Energy Build. 69, 122–130.
Cumby, T.R., 1987. A review of slurry aeration 2. Mixing and foam control. J. Agric. Eng. Res. 36 (3), 157–174.
Dogniaux, R., Lemoine, M., Sneyers, R., 1978. Année-type moyenne pour le traitement de problémes de capitation d'énergie solaire (Typical reference year for treatment of solar energy captation problems). Institut Royal Météorologique de Belgique, Bruxelles. Misc. sér. B, no. 45.
Dürrenmatt, D.J., Wanner, O., 2014. A mathematical model to predict the effect of heat recovery on the wastewater temperature in sewers. Water Res. 48, 548–558.
Fernandez-Arevalo, T., Lizarralde, I., Grau, P., Ayesa, E., 2014. New systematic methodology for incorporating dynamic heat transfer modelling in multi-phase biochemical reactors. Water Res. 60, 141–155.
Frenkiel, J., 1965. Evaporation Reduction: Physical and Chemical Principles and Review of Experiments. UNESCO, Paris.
Gillot, S., Vanrolleghem, P.A., 2003. Equilibrium temperature in aerated basins—comparison of two prediction models. Water Res. 37 (15), 3742–3748.
Harbeck Jr., G.E., 1962. In: A Practical Field Technique for Measuring Reservoir Evaporation Using Mass-transfer Theory Professional Paper.
Heymann, E., Yoffe, A., 1942. The stability of multimolecular films of hydrocarbon oils, containing spreaders, on water surfaces. Trans. Faraday Soc. 38, 408–417.
Heymann, E., Yoffe, A., 1943. The equilibrium between lens and unilayer in the system hydrocarbon oil-oleic acid-water in relation to the interfacial film. Trans. Faraday Soc. 39, 217–219.
Hughes, D.F., 1984. Extraction of energy from an aerobic farm waste lagoon. J. Agric. Eng. Res. 29 (2), 133–139.
Lippi, S., Rosso, D., Lubello, C., Canziani, R., Stenstrom, M.K., 2009. Temperature modelling and prediction for activated sludge systems. Water Sci. Technol. 59 (1), 125–131.
Makinia, J., Wells, S.A., Zima, P., 2005. Temperature modeling in activated sludge systems: a case study. Water Environ. Res. 77 (5), 525–532.
MATLAB R2014a, The MathWorks, Inc., Natick, Massachusetts, United States.
Meggers, F., Leibundgut, H., 2011. The potential of wastewater heat and exergy: decentralized high-temperature recovery with a heat pump. Energy Build. 43 (4), 879–886.
Novotny, V.A., Krenkel, P.A., 1973. Evaporation and heat balance in aerated basins. AICHE Symposium Series Water 70, 150–159.
Oke, T.R., 1992. Boundary Layer Climates, second ed. Routledge, New York.
Pieters, J.G., Deltour, J.M.J.J., Debruyckere, M.J.G., 1995. Onset of condensation on the inner and outer surface of greenhouse covers during night. J. Agric. Eng. Res. 61 (3), 165–171.
Raphael, J.M., 1962. Prediction of temperature in rivers and reservoirs. J. Power Div. ASCE 88, 183–192.
Sedory, P., Stenstrom, M., 1995. Dynamic prediction of wastewater aeration Basin temperature. J. Environ. Eng. 121 (9), 609–618.
Shukla, R.N., Deo, A.V., Sanjana, N.R., Kulkarni, S.B., 1962. The influence of temperature on the water evaporation retardation by monolayers. In: Paper Presented at the Unesco/CSIR Symposium on Water Evaporation Control, Poona, India.
Svoboda, I.F., Evans, M.R., 1987. Heat from aeration of piggery slurry. J. Agric. Eng. Res. 38 (3), 183–192.
Swinbank, W.C., 1963. Long-wave radiation from clear skies. Q. J. R. Meteorol. Soc. 89 (381), 339–348.
Talati, S.N., 1988. Heat Loss in Aeration Basins. University of California at Los Angeles, California (MSc).
Talati, S.N., Stenstrom, M.K., 1990. Aeration basin heat loss. J. Environ. Eng. 116, 70–86.
Wiesmann, U., 1994. Biological nitrogen removal from wastewater. Adv. Biochem. Eng. Biotechnol. 51, 113–154.